Generating Synthetic Turbulence in Astrophysical Plasmas

DESY Summer Student Programme, 2019

Jonas Sinjan

Imperial College London, UK

Supervisors
Dr. Kirit Makwana & Prof. Huirong Yan

September 4, 2019

Abstract

Two computational FORTRAN methods were considered to generate synthetic plasma turbulence data according to the Goldreich-Sridhar 1995 spectrum: the 'displacement' and 'squares' methods. These methods attempted to produce a scalar field that obeys the GS95 scaling with respect to the local mean magnetic field rather than the global field. Both were tested in 2D, with the displacement method further extended to 3D. The displacement method was shown to outperform the squares method. The displacement method produced a structure function however which did not agree with theory and could be due to several reasons, but the limiting factor for our analysis was the low resolution. Several tests were implemented to verify these methods which showed that the initialisation of the scalar field was performed correctly. To increase the resolution, the initialisation was performed in Fourier space, which was significantly more efficient than initialisation in real space. This initialisation gave better results at higher resolution, but still did not match theory perfectly and requires further investigation.

Imperial College London

DESY.

Contents

1   Introduction

There are currently many experiments studying cosmic rays and the particle showers they create upon interaction with the atmosphere. The study of cosmic rays is extremely important as it provides information about their sources; such as active galactic nuclei: black holes at the centre of galaxies[1]. The interstellar medium is mostly composed of astrophysical plasma, and the cosmic rays we study, propagated through this plasma on their journey to Earth. It is therefore key to understand the plasma's properties and how it affects these cosmic rays.

The astrophysical plasma in the interstellar medium can be very turbulent due to a variety of physical processes. Supernovae explosions, stellar winds and turbulent accretion flows around compact objects are three such examples of processes that are able to produce turbulence in plasmas. For perfect conductors, which we consider the plasma to be for this project, the magnetic field lines are 'frozen' into the plasma: this is Alfven's theorem, which originates from the MHD induction equation[2]. It is the interaction between the cosmic rays and these 'frozen-in' magnetic field that affects their propagation, via particle heating and acceleration, causing the cosmic rays to scatter and become isotropic[3].

The standard method to investigate MHD turbulence is to perform numerical simulations which directly solve the incompressible MHD equations. This is a very expensive simulation and one example of such a simulation is that performed by Hayes et al. (2006) wherein they perform an ideal 3D MHD turbulence numerical simulation of a 1024^3 cube which required $\sim 50,000$ CPU hours[4][5]. This is only worsened as the computational time for this simulation is increased at least 16-fold, when the resolution is doubled, because of the the accuracy constraint which requires the time step to be halved[5]. The aim of this project is to formulate a method to generate synthetic turbulence data much more cheaply. Such turbulence data can then be used to analyse cosmic ray propagation through turbulent magnetic fields. To achieve this we use a theory by Goldreich-Sridhar, published in 1995, wherein they describe a model with anisotropic MHD turbulence[6]. A key point from this theory is that the turbulence is dependent on the local mean magnetic field, rather than the global one. For example, a supernovae explosion, which could cause the plasma turbulence, can create a disturbance on a scale of approximately 100 parsec, however the magnetic field that a cosmic ray experiences, when it passes through the ISM, could be on a scale much less than the supernovae, like 0.1 parsec. This is an example of why it is important to consider the local mean magnetic field when creating synthetic turbulence data.

2 Theory & Methods

2.1 Goldriech-Sridhar 1995

The most widely accepted theory of astrophysical turbulence is the Goldreich-Sridhar 1995 theory[6]. For example, their theory was shown to be consistent with analysis from the Ulysses satellite when it recorded measurements of the solar wind magnetic field[7]. Their theory describes an anisotropic model under a strong turbulence limit where it is assumed that the interstellar medium is filled with Alfvén waves[8]. In their model, a system of two wave packets, travelling along the magnetic field lines towards each other, is described. Their interaction and corresponding distortion is modelled. They solve for two equations between which a critical balance must be maintained:

$$v_\lambda \sim \frac{\epsilon^{1/3}}{k_\perp^{1/3}}, \tag{1}$$

and

$$k_\parallel v_A \sim \epsilon^{1/3} k_\perp^{2/3}, \tag{2}$$

where v_λ is the velocity of a wave packet, ϵ is the rate of energy transfer from a wave packet to larger $k_\perp$ and v_A is the velocity of the Alfvén waves. Here $k_\parallel$ and $k_\perp$ are the wave vectors parallel and perpendicular respectively to the local mean magnetic field. A balance must be held between v_λ and $k_\parallel$ as otherwise the number of required interactions to transfer energy to the next smaller scale would become less than one, which is implausible[8]. Equation 2 is a key result from this theory and provides an important scaling relation, between $k_\parallel$ and $k_\perp$, that can be used to verify the accuracy of the computational models that would generate the synthetic data.

Their model also predicts a spectrum for the turbulence in 3D[9]:

$$E(k_\parallel, k_\perp) = k_\perp^{-10/3} \exp\left(-\frac{k_\parallel}{k_\perp^{2/3}}\right), \tag{3}$$

where $E^{1/2}$ is the amplitude of the waves, $k_\perp$ and $k_\parallel$ are the perpendicular and parallel components of the wave vector respectively w.r.t the local mean magnetic field. When the energy spectrum, E, is integrated separately over $k_\perp$ & $k_\parallel$ the following relations are found:

$$E(k_\perp) \propto k_\perp^{-5/3}, \tag{4}$$

and

$$E(k_\parallel) \propto k_\parallel^{-2}. \tag{5}$$

These relations can also be used to test the computational methods' accuracy.

The scalar field, Φ, can be initialised in real or k-space:

$$\Phi(\underline{r}) = E^{1/2} cos(\underline{k} \cdot \underline{r} + \psi) \iff \widetilde{\Phi}(\underline{k}) = E^{1/2} \exp(i\psi), \tag{6}$$

where ψ is a random phase. Here we are initialising the above spectrum using $k_\parallel$ & $k_\perp$ w.r.t. the global mean field. The challenge is to produce a GS95 spectrum, equation 3, w.r.t. the local mean magnetic field. For this we describe two methods that had been implemented in FORTRAN in 2D: Squares and Displacement.

2.2   Squares Method

The first method is a simple procedure where the scalar field is first initialised with respect to the global frame. Then the domain is divided into smaller areas, and a scalar field is created in each of these regions with respect to the local mean magnetic field in these regions. These new scalar fields are then added to the initial field in their respective regions. This process is repeated by continually splitting the domain into smaller and smaller regions and adding a scalar field component from each subsequent division to the total field. This process is illustrated in figure 1 below.
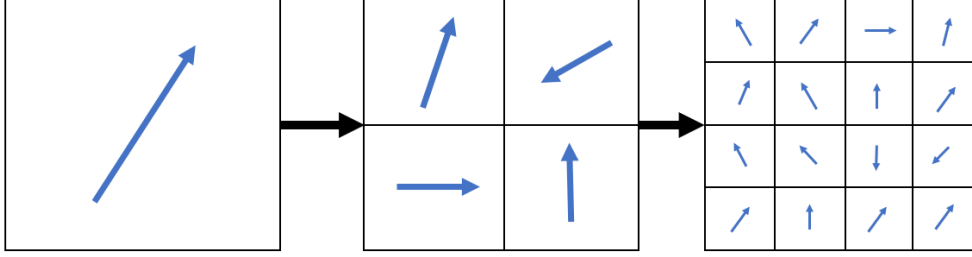

Figure 1: Domain split up into smaller areas, scalar field set according to local mean magnetic field. Keep splitting until Nyquist Frequency reached.

This requires some trial and error as the range of wave numbers used to create the scalar fields in each region is arbitrary.

2.3   Displacement Method

This method works by calculating the deviation of the local magnetic field from a uniform magnetic field and using this deviation to calculate the displacement of each point in the scalar field to deform it to produce a spectrum w.r.t. the local mean magnetic field. An illustrative example is shown below in figure 2.
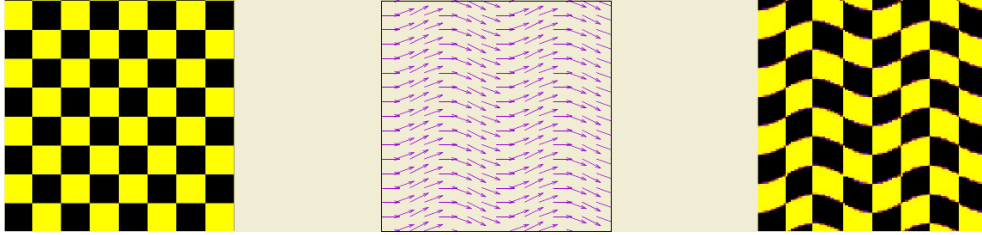

Figure 2: Given an initial scalar field (left) and a magnetic field (centre), the scalar field should be deformed to follow the magnetic field (right).

The method is performed as follows[10]: First a set of magnetic field distributions, $\widetilde{\mathbf{B}}^{(i)}(r)$, is made in Fourier space using spectral filtering:

$$\widetilde{\mathbf{B}}^{(i)}(r) = \langle \widetilde{\mathbf{B}}^{(i+1)}(r) \rangle_{k>k_i}, \tag{7}$$

where i denotes a particular distribution, n is the resolution and $\langle \rangle_{k>k_i}$ filters all frequencies $k > k_i$ where:

$$k_i = \sqrt{2} \cdot 2^{n-i}, \tag{8}$$

and $2^n = n_x = n_y = n_z$, where n_x is the number of grid points along the x-direction and n is a free parameter. It is important to clarify that in real space $\mathbf{B}^{i=0}(r)$ corresponds to the global mean magnetic field. As the index, i, increases, the magnetic field distribution corresponds to smaller wave numbers, which reveals the small scale structure . The reason for these sets of distributions is to define a range of scales for the displacement. In an ideal scenario, the displacement would be calculated at every scale, however that is impractical as it would be too computationally expensive. The choice for k_i is somewhat arbitrary, which introduces an element of trial and error into the method.

Now consider the MHD induction equation for a perfect conductor:

$$\frac{\delta \mathbf{B}}{\delta t} = \nabla \times (\mathbf{v} \times \mathbf{B}), \tag{9}$$

where $\mathbf{B}$ is the magnetic field and $\mathbf{v}$ is the velocity. Making an ansatz, this becomes:

$$\mathbf{B}^{(i+1)} - \mathbf{B}^{(i)} = \nabla \times (\delta \xi^{(i)} \times \mathbf{B}^{(i)}), \tag{10}$$

where $\delta \xi^{(i)}$ is the spatial displacement. This is transformed into k-space and solved for $\delta \widetilde{\xi}_*^{(i)} \equiv \delta \widetilde{\xi}^{(i)} \times \mathbf{B}^{(i)}$:

$$\delta \widetilde{\xi}_*^{(i)} = -\frac{1}{k^2} \left[\left(\widetilde{\mathbf{B}}^{(i+1)} - \widetilde{\mathbf{B}}^{(i)} \right) \times i\mathbf{k} \right] \tag{11}$$

A second ansatz is made:

$$\delta \xi_*^{(i)} = \delta \mathbf{R}^{(i)} \times \mathbf{B}^{(i)}, \tag{12}$$

where $\delta \mathbf{R}^{(i)}$ is the displacement field. This ansatz however requires that:

$$\delta \widetilde{\xi}_*^{(i)} \cdot i\mathbf{k} = 0. \tag{13}$$

From equation 12, the total displacement, $\Delta \mathbf{R}(\mathbf{r})$, for each point, $\mathbf{r}$, can be calculated:

$$\Delta \mathbf{R}(\mathbf{r}) = \sum_i \delta \mathbf{R}^{(i)}(\mathbf{r}). \tag{14}$$

Finally, the scalar field at each point, $\Phi(\mathbf{r})$, is deformed to its new position:

$$\Phi'(\mathbf{r}') = \Phi(\mathbf{r} + \Delta \mathbf{R}). \tag{15}$$

2.4 Magnetic Field Perturbation

An average magnetic field was setup with $\mathbf{B}_{0x} = 1$, $\mathbf{B}_{0y} = 0$, and $\mathbf{B}_{0z} = 0$ for 3D. This defines the global reference frame of the magnetic field: $\mathbf{B}_0$. A perturbation of the magnetic field was added for both the squares and displacement methods, ensuring that the average magnetic field was unchanged. Therefore a sinusoidally varying field was added in the B_y direction in both 2D and 3D:

$$B_y = 0.5 sin(2x). \tag{16}$$

2.5   Structure Function

An important measure of performance of these methods is the structure function, which depends on the scale of the turbulence in real space: $l_\perp$ and $l_\parallel$ w.r.t. the local mean magnetic field. The anisotropic structure function, SF, is defined as follows w.r.t the local mean magnetic field:

$$SF(l_\parallel, l_\perp) = \langle (\mathbf{B}(r + l_\parallel \hat{b}_\parallel + l_\perp \hat{b}_\perp) - \mathbf{B}(r))^2 \rangle, \tag{17}$$

where $\mathbf{B}$ is the magnetic field and r is a randomly selected point. At r the local magnetic field and its direction is found by averaging the magnetic field within a sphere of radius $l = \sqrt{l_\parallel^2 + l_\perp^2}$. A point, a distance $l_\parallel$ away along the local field direction and distance $l_\perp$ away in the perpendicular direction, is then identified and the difference in the magnetic field between these two points is calculated and squared. The average of this value is found by performing this operation between many pairs of points. From one of the key results from GS95, equation 2, a relation between $l_\perp$ and $l_\parallel$ can be found:

$$l_\parallel \propto l_\perp^{2/3}. \tag{18}$$

This is due to the fact that $k \propto 1/l$, so therefore the same relation, equation 2 applies for $l_\perp$ and $l_\parallel$, as used in the structure function. This relation implies a slope of 2/3 on a logarithmic plot.

3   Results and Discussion

3.1   Initial Results

3.1.1   Displacement vs. Squares

Firstly, the two methods were executed in 2D and output a final scalar field, denoted as Φ. The displacement method for this configuration initialised Φ_0 in real space. This scalar field was then used to calculate the 2D anisotropic structure function which is dependent on $l_\parallel$ and $l_\perp$, as described in section 2.5. The limiting factor of the highest resolution possible for equal comparison, was the displacement method, as for it to execute in a practical time-frame (i.e. maximum a couple of hours) a resolution of 512^2 was used. The squares method executed much faster as it initialised Φ_0 in k-space: $\widetilde{\Phi}_0$ (equation 6), which greatly increased the speed of the computation. The structure function using Φ from both methods with a 512^2 resolution was plotted and shown below in figure 3.
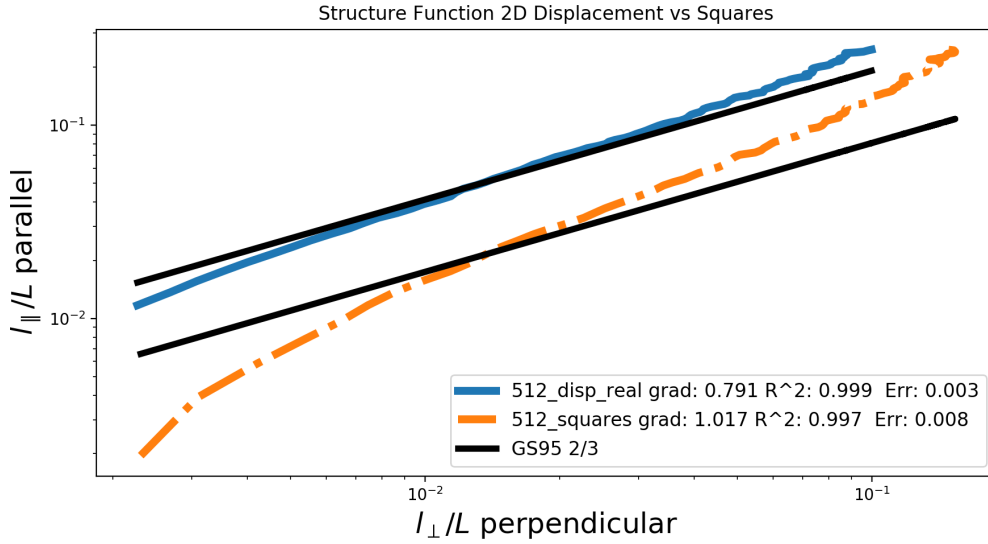

Figure 3: Plot of the 2D anisotropic structure function of the output scalar field: PHI, comparing Displacement vs Squares method in 2D. These methods both used a 512^2 resolution. Here it was clear that the displacement method outperformed the squares method.

This figure shows that the displacement method produced a scalar field, Φ, which had a spectrum which aligned closer to the GS95 spectrum than that produced by the squares method. It is for this reason that the displacement method was chosen to be extended to 3D.

3.1.2   2D vs 3D Displacement

The displacement method, initialising Φ_0 in real space, was extended to 3D. However the extra dimension greatly increased the computational time required. A 128^3 resolution in 3D was completed in 43 hours. This was because to double the resolution, the computational time required was multiplied by approximately 2^6. This is because to create Φ_0, a 6 nested for loop was required, the three wave vectors in all dimensions, followed by the Cartesian

coordinates, x, y, z, as described in equation 6. The structure function of the displacement methods in 2D and 3D is plotted below in figure 4.
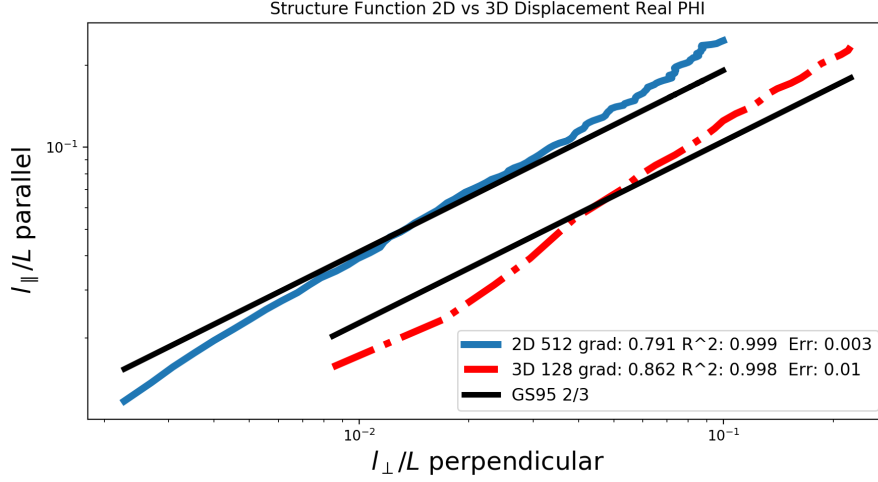

Figure 4: Plot of the 2D anisotropic structure function of the output scalar field: Φ, comparing Displacement in 2D and 3D. Here it is clear that the 3D method produces a spectrum similar to 2D, however it was restricted by its low resolution of only 128^3 while the 2D method had a resolution of 512^2.

It is shown here that the displacement method was successfully extended to 3D, however it was clear that this model produced a less accurate spectrum. This was mainly due to the fact that the resolution of the 3D model was much lower. To perform any meaningful simulations the method must be made faster to access higher resolutions. It is clear however, that in both these figures: figures 4 & 3, the spectra produced a structure function which was different from that implied by equation 2. It was therefore necessary to verify the method.

3.1.3   Displacement Method Verification

As described in equations 4 and 5, the GS95 spectrum obeys two power laws. The integrated spectra is plotted against its respective k to investigate if the initialisation of Φ: Φ_0, was performed correctly, as shown below in figure 5. These plots imply that the initialisation in real space was performed as intended. It is important to note however that these power laws do not hold for all scales, and the region to perform the linear fit must be found by inspecting the spectra over all scales. This revealed that the discrepancy of the structure function from a slope of 2/3 appeared to originate elsewhere. There are several areas where this could have arisen from, first of all the displacement method could be implemented incorrectly or the structure function could be incorrectly calculated. Moreover, the requirement to make the second ansatz, as described in section 2.3 by equation 13, could be a source of error, as this assumption might be invalid to make and therefore have to be modified. This would need to be investigated further. Furthermore these spectra also depended on the initial magnetic field perturbation setup in equation 16. The spectra that resulted from these methods should be investigated to determine how they vary for different magnetic field perturbations, i.e. changing M_A, the Alfénic Mach number[11].
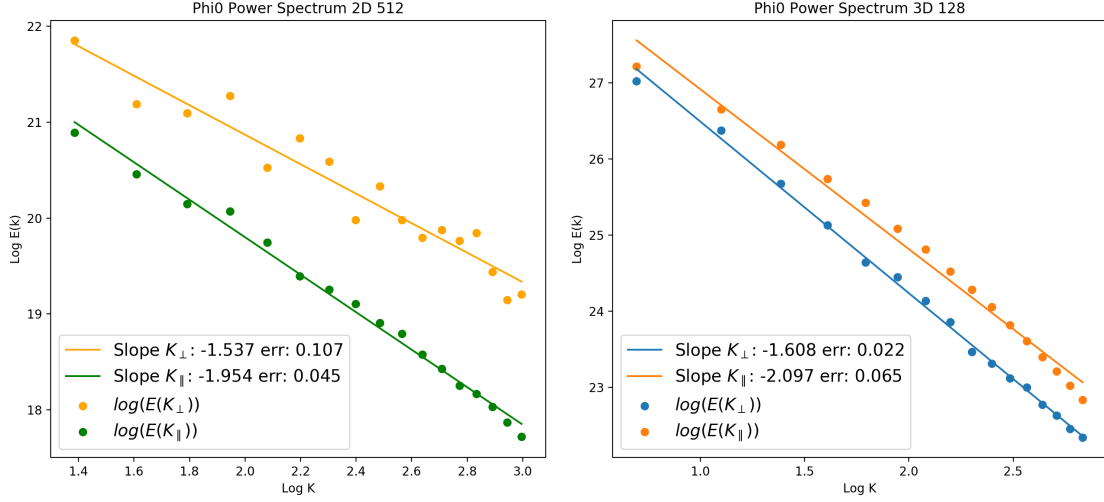
Figure 5: Left: Power Spectrum 2D 512^2 Φ_0; Right: Power Spectrum 3D 128^3 Φ_0. The slope found by linear regression is close to the explicit values of $-5/3$ and -2.

3.2   K Space Displacement Method

To reduce the computational time the initialisation of Φ, Φ_0, was performed instead in k space (equation 6), and then inverted back into real space using the inverse discrete fast fourier transform in FORTRAN. For simplicity, this method will now be referred to as the 'FFT' method and that the method in section 3.1.1, where the initialisation of Φ was performed in real space as the 'real' method. This greatly reduced the computational time for 3D 128^3 from 43 hours to ~ 4minutes.

3.2.1   Real vs FFT 3D

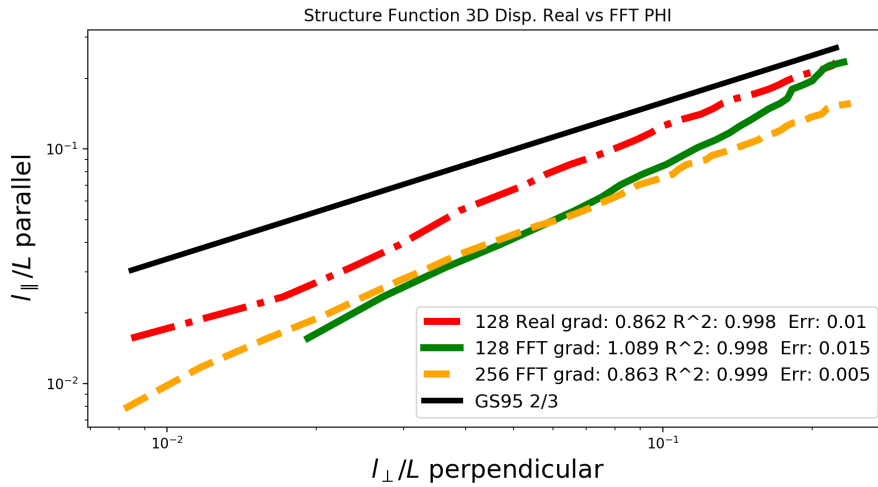Firstly, the FFT method in 3D was compared to that produced by the real 3D method, as shown in figure 6.

Figure 6: Plot of the 2D anisotropic structure function of the output scalar field: Φ, comparing 3D Displacement with real and FFT Φ_0 initialisation with different resolutions.

This figure displays that the 128^3 FFT scalar field produced a structure function that varied further from a slope of 2/3 than that from 3D 128^3 scalar field. This was an interesting result that is not fully understood. In an effort to further investigate this the FFT method resolution was increased to 256^3, which produced a structure function very similar to that from the real 128^3 method. This also shows that as the resolution increases, the slope of the structure function matched theory more closely. A 512^3 simulation was not possible as the program required too much RAM, at least $\sim 50GB$ was required for 512^3 which was not possible to run on the available computing infrastructure. Therefore the programs need to be made more memory efficient, to access higher resolutions.

3.2.2   FFT Verification

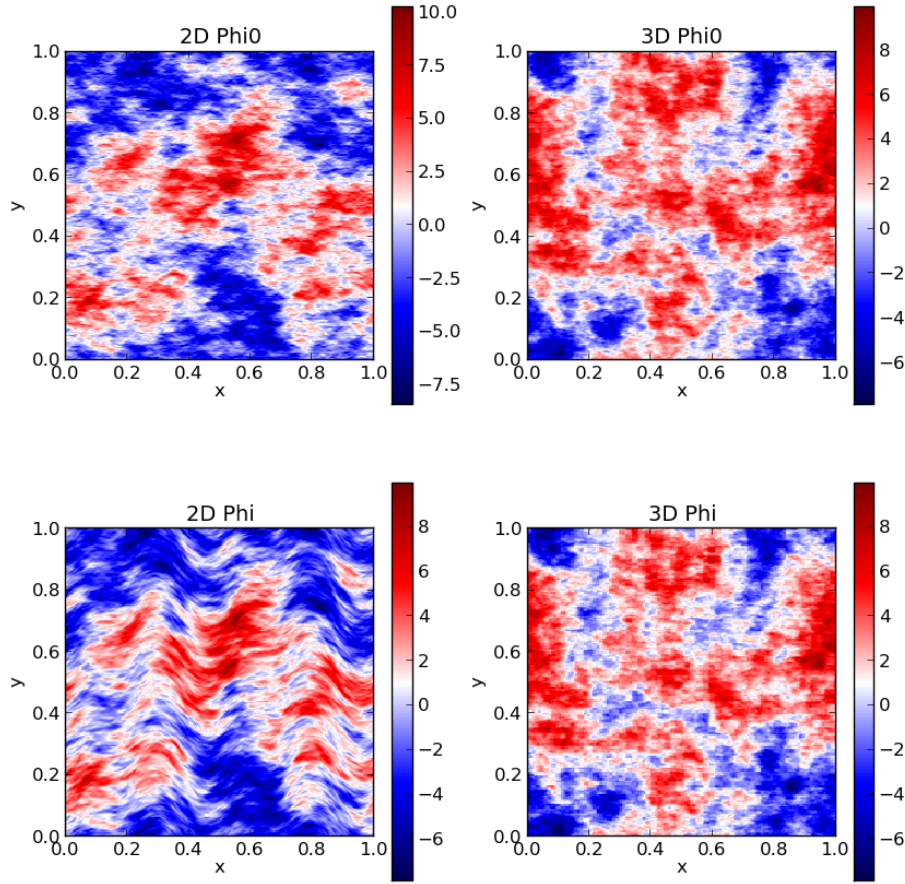A test of the displacement method was performed by visually inspecting Φ. This is shown in figure 7 below.

Figure 7: Plot of X,Y Slices of Φ_0 and Φ for 2D and 3D FFT methods.

The plot for 2D Φ_0 indicated that a random field with structures elongated in the x direction were created and it is clearly demonstrated that the sinusoidal variation from the magnetic field in Φ was present, indicating that the displacement method deformed the initial field correctly. However this was not present in the 3D plots. It was difficult to spot, but there were subtle changes between the plot for Φ_0 and Φ, showing that this method did have an effect on the initial scalar field, however it was extremely minimal. This result

was not understood and needs to be investigated further. As in section 3.1.3, the K space initialisation was verified by investigating the power spectrum of Φ_0, as shown below in figure 8.
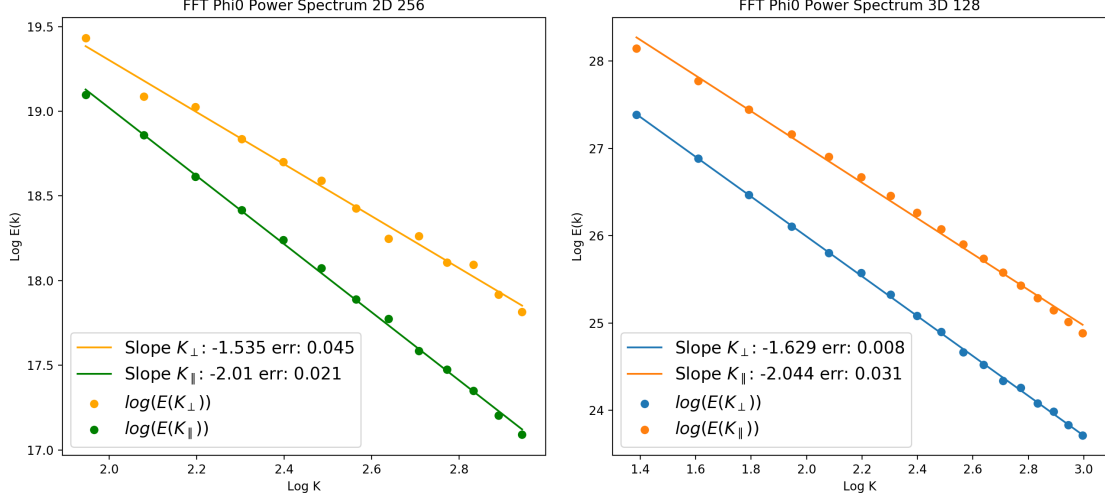

Figure 8: Left: Power Spectrum FFT 2D 512^2 Φ_0; Right: Power Spectrum FFT 3D 128^3 Φ_0. The slope found by linear regression is close to the explicit values of $-5/3$ and -2.

These plots confirm that the k space initialisation was performed correctly and thus more investigation is required to determine why in 3D the displacement method seemed to work less accurately.

4   Conclusions

The displacement method in 2D was shown to outperform the squares method for a resolution of 512^2. The displacement method was extended to 3D and the Φ_0 initialisation procedure was verified using the power law relations predicted by the GS95 theory. Nevertheless, the structure functions from the displacement method in 2D & 3D did not match theory perfectly and needs to be further investigated. The limiting factor for this analysis was the low resolution in 3D: 128^3, to overcome this the initialisation procedure was completed in fourier space: the FFT method, greatly reducing the computational time for 128^3 from 43 hours to ~ 4 minutes. However a resolution of 512^3 was not possible as the program required too much RAM and thus needs to be made more memory efficient. The structure function with the FFT method was worse for 128^3 but that from 256^3, matched the structure function from 128^3 using the real space initialisation. To access higher resolutions it is recommended that the FORTRAN methods be ported to python and use the MPI4py package to safely parallelise the programs and decrease the computational time. Finally, the 3D results should be compared for a varying M_A, Alfvénic mach number, to study how the method performs for different magnetic fields.

Acknowledgements

I would like to thank my supervisors, Dr. Kirit Makwana and Prof. Huirong Yan for their guidance throughout my project. I would also like to thank DESY and in particular DESY-Zeuthen for this opportunity. Finally, I would like to thank Gernot Maier and the administration team for making this summer student program possible.

References

[1] Terry Devitt. What are cosmic rays? Why do they matter? University of Wisconsin News. https://news.wisc.edu/what-are-cosmic-rays-why-do-the-matter/.

[2] Hannes Alfvén. Existence of electromagnetic-hydrodynamic waves. *Nature*, 150(3805):405, 1942.

[3] Reinhard Schlickeiser. *Cosmic ray astrophysics*. Springer Science & Business Media, 2013.

[4] John C Hayes, Michael L Norman, Robert A Fiedler, James O Bordner, Pak Shing Li, Stephen E Clark, Mordecai-Mark Mac Low, et al. Simulating radiating and magnetized flows in multiple dimensions with zeus-mp. *The Astrophysical Journal Supplement Series*, 165(1):188, 2006.

[5] Pak Shing Li, Daniel F Martin, Richard I Klein, and Christopher F McKee. A stable, accurate methodology for high mach number, strong magnetic field mhd turbulence with adaptive mesh refinement: resolution and refinement studies. *The Astrophysical Journal*, 745(2):139, 2012.

[6] P Goldreich and S Sridhar. Toward a theory of interstellar turbulence. 2: Strong alfvenic turbulence. *The Astrophysical Journal*, 438:763–775, 1995.

[7] Miriam A Forman, Robert T Wicks, and Timothy S Horbury. Detailed fit of "critical balance" theory to solar wind turbulence measurements. *The Astrophysical Journal*, 733(2):76, 2011.

[8] Russell M. Kulsrud. *Plasma physics for astrophysics*. Princeton University Press, 2005.

[9] Jungyeon Cho, Alex Lazarian, and Ethan T Vishniac. Simulations of magnetohydrodynamic turbulence in a strongly magnetized medium. *The Astrophysical Journal*, 564(1):291, 2002.

[10] Michael Vorster. *Synthetic Turbulence note, by private communication*. DESY Zeuthen.

[11] Benjamin M Tofflemire, Blakesley Burkhart, and A Lazarian. Interstellar sonic and alfvenic mach numbers and the tsallis distribution. *The Astrophysical Journal*, 736(1):60, 2011.